Biomedical Engineering Advances 7 (2024) 100123

Contents lists available at ScienceDirect

Biomedical Engineering Advances

journal homepage: www.journals.elsevier.com/biomedical-engineering-advances

Investigating the impact of contact pressure on photoplethysmograms

Jukka-Pekka Sirkiä *, Tuukka Panula, Matti Kaisti

Department of Computing, University of Turku, Vesilinnantie 5, 20500 Turku, Finland

ARTICLE INFO

Keywords:
Photoplethysmography
Contact pressure
Peripheral oxygen saturation
Pulse arrival time
Pulse wave analysis

ABSTRACT

Photoplethysmography (PPG) sensors are widely used to measure a variety of physiological parameters, from heart rate to clinically important peripheral oxygen saturation (SpO_2). The ease of obtaining a PPG signal simply by placing the sensor on a body site with even remotely sufficient vasculature (typically the wrist, finger, earlobe, or temple) can easily lead to overlooking the aspect of appropriate sensor contact pressure (P_c). We sought to investigate the effects of P_c from the perspective of: (i) SpO_2, (ii) pulse arrival time (PAT), and (iii) PPG features. Consequently, we developed a finger cuff device to measure multispectral (green, red, and infrared (IR)) PPG signals at different P_c levels. The SpO_2 values were found to increase, driven by the IR component, above the theoretical maximum of 100% slightly after the level of the mean arterial pressure. The maximum variation due to P_c was approximately 1.9 percentage points. PAT values calculated using the waveform feet of the red and IR channels were the most robust. PPG features were also sensitive to varying sensor P_c levels, with each feature showing a rather unique response. However, in general, a P_c between 20–30 mmHg (a slight P_c) and the level of diastolic blood pressure is likely to produce the best results on the features. Overall, the results showed that sensor P_c is a source of inaccuracy in PPG analysis and therefore should be given more consideration in device designs.

1. Introduction

Photoplethysmography (PPG) is an optical technique to measure changes in blood volume within the skin with a wide range of applications, from simple heart rate measurement to clinical pulse oximeters. PPG sensors are extensively used in modern wearables (e.g., smart rings and smart watches, and in the future in patch form factor) because they are easy to use: A body site with even remotely sufficient vasculature is all that is needed to obtain a PPG signal. This can easily lead to overlooking sensor contact pressure (P_c) in device designs, and, in fact, best practices with respect to P_c have yet to be established [10,40,49,51,52]. The impact of P_c on PPG signals is therefore still an open question that requires more research to understand how the signals and the various parameters calculated from them change as P_c is varied. This is especially important in PPG applications that aim to measure clinically important parameters, such as oxygen saturation and, more recently, blood pressure (BP).

A PPG sensor uses a light source to illuminate the skin and a photodetector to record light backscattered from the tissue. The recorded signal consists of AC (pulsatile) and DC (nonpulsatile) components, of which the former is synchronized with the activity of the heart and the latter is related to the average blood volume and tissues [2,28]. PPG signal analysis uses these two components to compute parameters from the different fiducial points of the waveform (a single pulse in the AC component) or its derivatives, the baseline (the DC component) or a combination of parameters computed from the waveform and the baseline [2,16,28]. Both the shape of the waveform and the baseline are known to be affected by the P_c [27,47,53] as well as the parameters calculated from these, such as the pulse arrival time (PAT) [8,54].

Detailed studies demonstrating the effects of P_c on PPG signals date at least to the 1970s and 1980s [57–59]. Pressure cuff-based oscillometric measurements showed that the maximum amplitude of the infrared (IR) PPG AC component closely corresponds to mean arterial pressure (MAP) [57,59]. That particular point (i.e., MAP) is also known as the point where the transmural pressure, $P_t = P_a - P_{ext}$ (pressure inside the artery minus external pressure), reaches zero and where arterial compliance reaches its maximum (the vascular wall is in an unloaded state) [36,51,57,59]. The initially increasing and subsequently decreasing AC amplitude has since been shown in several experimental studies [21,24,46,53]. Experiments with a tissue phantom have revealed that increasing P_c also changes, for example, the pulse area and the angle and rise time of the systolic phase [27]. These are typical features used in

* Corresponding author.
E-mail address: jpsirk@utu.fi (J.-P. Sirkiä).

https://doi.org/10.1016/j.bea.2024.100123
Received 17 November 2023; Received in revised form 28 March 2024; Accepted 8 April 2024
Available online 15 April 2024

pulse waveform analysis (PWA), which is increasing in popularity, driven by the use of artificial intelligence. PWA is currently heavily researched, especially in the area of estimating BP from the PPG waveform (e.g. [44]). In addition to BP, the PPG waveform has been studied, for example, in vascular age assessment [9], signal quality assessment [38], atrial fibrillation detection [5], pregnancy monitoring [6], and postoperative pain assessment [60]. Regarding the DC component, it has been shown to increase with increasing P_c [21,53,58].

Recent studies on multi-wavelength PPG (MWPPG) have shown that the response to P_c is wavelength-dependent. For example, the amplitude of a green PPG signal reaches its maximum at a lower pressure reading than the amplitude of an IR PPG signal [24,46,47]. This is because the penetration depth of light depends on the wavelength [34], with longer wavelengths probing larger, higher pressure, arteries deep in the skin, while shorter wavelengths probing more superficial, lower pressure, blood vessels.

Studies on P_c and PAT, that is, the time difference between a PPG fiducial point (e.g. the waveform foot) and the electrocardiogram (ECG) R peak, which is another line of research to develop a cuffless BP method, have produced varying results. The experimental and subsequent theoretical analysis in [54,55] showed that PAT increases in the positive P_t region before plateauing in the negative P_t region. Different results were obtained in [8] where the experimental measurements resulted in a decrease in PAT in the positive P_t region and an increase in PAT in the negative region. However, the comparison of the results is not straightforward, as in [54,55] P_t was defined using the maximum amplitude of PPG (which closely corresponds to MAP), while in [8] it was defined relative to diastolic BP (DBP). Moreover, the fiducial points of the PPG waveform differed in [54] from the two other studies.

Despite the diagnostic importance of the pulse oximeter, studies on P_c and peripheral oxygen saturation (SpO_2) seem to be surprisingly scarce. In [22] tests with a custom fingertip PPG setup resulted in an optimal P_c between 5–15 kPa (≈ 38–113 mmHg). Similar pressure levels were reported in [15] where the variability of the red-IR light intensity ratio was found to decrease when pressure between 55 and 90 mmHg was applied to a PPG sensor on the forehead. It was hypothesized that the applied pressure blocked venous blood from interfering while simultaneously increasing pulse amplitudes [15]. The benefit of venous blocking was also hypothesized in [43] where application of pressure on the forehead sensor resulted in cleaner signals. In [39] P_c was generally found to affect SpO_2 with the conclusion that SpO_2 decreases with increasing P_c.

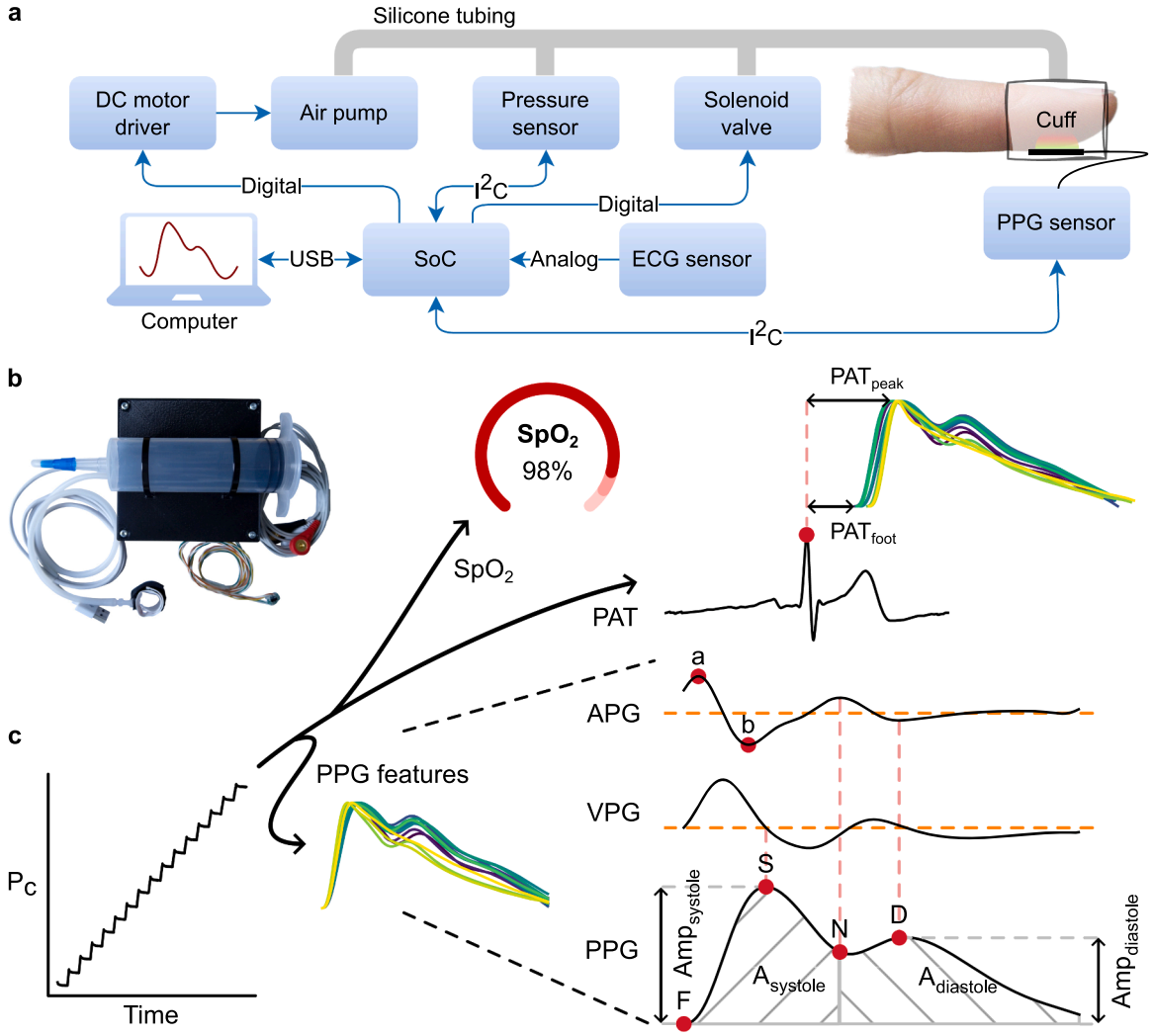

Fig. 1. The developed device and the performed experiment. a. System block diagram showing the main components. b. Picture of the device. c. Illustration of the experiment in which the effects of increasing P_c on SpO_2, PAT, and PPG features are investigated. The labels next to *PPG features* are: i) PPG derivative waveforms: first derivative (VPG) and second derivative (APG); ii) APG waveform points a (a) and b (b); iii) PPG waveform fiducial points: systolic peak (S), diastolic peak (D), dicrotic notch (N), and foot (F); iv) PPG waveform features: systolic and diastolic amplitudes ($Amp_{systole}$ and $Amp_{diastole}$) and respective waveform areas ($A_{systole}$ and $A_{diastole}$). The horizontal orange dashed lines mark the derivative zero lines. The vertical dashed lines illustrate how S, N, and D have been detected using the VPG/APG waveforms.

The mounting evidence of the impact of P_c on PPG signals has led to different experimental devices that take P_c into account [14,37,41,45]. This study further investigates the effects of PPG sensor P_c on (i) the clinically important SpO_2, (ii) PAT and (iii) PPG features (used, e.g., in PWA), with the latter two being currently very relevant, as they are indeed heavily researched with the aim of developing a cuffless BP measurement technique. Consequently, we developed a finger cuff device integrating a three-channel (green, red, and IR) PPG sensor and an ECG sensor, and performed measurements in which external pressure increased in steps of 10 mmHg. From now on, we will use the term P_c to refer to the pressure at which the PPG sensor presses the skin (i.e., $P_c \approx$ external pressure $\approx$ cuff pressure). Thus, the relationship between P_t and P_c is: $P_t = P_a - P_c$, with P_a assumed to be equal to MAP. The developed measurement system is presented in Fig. 1a and Fig. 1b. The experiment performed is visualized in Fig. 1c.

2. Methods

2.1. Hardware

The device is controlled by ESP32-S3 (Espressif Systems, China), which is a dual-core (maximum clock speed of 240 MHz) system-on-chip (SoC) with a comprehensive set of peripherals. The analog-to-digital converter (ADC) of the chip digitizes the analog signal generated by an ECG sensor (AD8232 by Texas Instruments, USA) while the I^2C serial communication is used to interact with a reflectance-mode PPG sensor (MAX30101 by Maxim Integrated, USA) and a pressure sensor (MPRLS0025PA00001A by Honeywell, USA).

The MAX30101 PPG sensor is a compact three-channel (537 nm, 660 nm, and 880 nm) module that incorporates all the circuits required to drive light-emitting diodes (LEDs) and digitize a photodiode signal. The LEDs and the photodiode are next to each other, separated by an optical barrier with a source-detector distance of approximately 3 mm. The sensor has ambient light cancellation and a digital filter, but no automatic gain control that could affect the measured signals in terms of amplitudes. The included digital filter is proprietary, but the effect of filtering on the PPG waveform is likely to be very small.

The pressure sensor measures the internal pressure of a custom-made finger cuff, which was made by cutting a piece from a wrist cuff and then sealing it together with a heat sealer. The cuff pressure is increased with an air pump (PUMP-924B by Transtek Medical, China) by controlling its 3 V DC motor through a motor driver (TB6612FNG by Toshiba Corporation, Japan). The pump flow rate was found to be slightly too high for the small finger cuff, and therefore the air volume was increased with a 100 ml syringe to decrease the fill rate of the cuff. That is, increasing the total air volume results in slower filling of the cuff with constant pump flow rate and thus more gentle changes in signals between the pressure steps. A miniature 3 V solenoid valve (JQF1-3A, generic brand) is used to release the cuff pressure.

The finger cuff, pressure sensor, air pump, syringe, and solenoid valve are connected to each other with silicone tubing. The sampling frequency is 100 Hz for all signals. All three channels – green (537 nm), red (660 nm) and IR (880 nm) – of the PPG sensor were used.

2.2. Software

The device firmware was programmed in C language using the Espressif Internet of Things (IoT) development framework known as ESP-IDF. The firmware is responsible for sampling the sensors and controlling the pump and solenoid valve. In order to extract SpO_2 data from the recorded PPG signals, the SpO_2 algorithm published by Maxim Integrated in their Arm Mbed repository [35] was integrated into the firmware.

A graphical user interface was developed in Python using the PyQt6 toolkit to control the device and visualize the signals in real time. The recorded signals are stored by the program as a comma-separated value file on the computer for later analysis. The analysis code was also written in Python.

2.3. Signal processing

The recorded signals were upsampled using third order spline interpolation to a sampling frequency of 500 Hz to gain better temporal resolution. The AC and DC components of the PPG signals were extracted using 4^{th} order zero-phase Butterworth bandpass and lowpass filters, respectively, with cutoff frequencies set to [0.5, 10.0] (bandpass filter) Hz and 0.5 Hz (lowpass filter). The AC components were then flipped so that the systolic peaks pointed up. The AC components of the ECG signals were extracted using the same filter construction, but with the bandpass filter cutoff frequencies set to [0.5, 40] Hz. The PPG feet and peaks were detected with the automatic multiscale-based peak detection (AMPD) algorithm [42]. ECG R peaks were detected with the Pan-Tompkins algorithm [30].

2.3.1. Peripheral oxygen saturation

The Maxim algorithm integrated into the firmware was used to calculate and record the following ratio used in SpO_2 estimation:

$$R = \frac{AC_{red}/DC_{red}}{AC_{IR}/DC_{IR}}, \tag{1}$$

where *AC* and *DC* refer to the respective AC and DC components of the red and IR PPG signals. In the embedded software, the ratio was calculated using five-second long data buffers. In the analysis phase, post measurements, the Equation 1 was computed using the detected waveform feet and peaks and the extracted DC components of the red and IR channels. Waveform amplitudes were simply calculated as the difference between waveform values at the peak and foot locations. The DC level was calculated as the mean value over the duration of the waveform. The amplitudes and DC levels of the red and IR signals were matched by finding the IR waveform foot closest to a red waveform foot within $\pm$100 ms. That is, the result was an array of R values with locations that corresponded to the red waveform feet. SpO_2 was then calculated using the equation used by the PPG sensor manufacturer [19]:

$$SpO_2 = aR^2 + bR + c, \tag{2}$$

where $a = 1.5958422$, $b = -34.6596622$, and $c = 112.6898759$. As a side note, the MAX30101 sensor is suitable for both finger and wrist based applications. [19] The arrays of R and SpO_2 values were then interpolated to the length of the entire signal using the previous value as the interpolated value. The R values computed post measurements were very close to the values computed by the embedded Maxim algorithm. Because the self-computed values provide better temporal resolution (computed over each PPG waveform vs. 5-second buffer), they were used in the final analysis.

2.3.2. Pulse arrival time

PATs were calculated using the detected ECG R peaks and both the PPG waveform feet and peaks. PPG feet and peaks were matched with the R peaks for each PPG channel by using thresholds that define the minimum and maximum distances allowed after an R peak. For the feet, the thresholds were [150, 400] ([minimum, maximum]) ms for the green channel and [150, 300] ms for the red and IR channels. Similarly, for the peaks, the thresholds were [300, 600] ms and [300, 500] ms, respectively. The resulting arrays of PAT values aligned with the R peak locations were then interpolated to the length of the entire signal using the previous value as the interpolated value.

2.3.3. Photoplethysmogram features

The calculated AC components were normalized to the range [0, 1]. Average waveforms were extracted for each 10 mmHg pressure step

using waveform feet. Then each average waveform was shifted with respect to the y-axis by subtracting its minimum value from each sample, and the time axis was normalized to have a unit length to reduce heart rate dependence. In addition, the amplitudes were also normalized to unity except, of course, for the amplitude feature. The first and second derivatives, known as the velocity plethysmogram (VPG) and the acceleration plethysmogram (APG) [32], were calculated from the average waveform using a 7^{th}-order Savitzky-Golay filter with a window length of 11 [17]. The location of the systolic peak was defined as the point at which the VPG turns negative the first time. The location of the diastolic peak was identified from the APG using the location of the first negative local minimum after the highest local maximum within 30% of the waveform length from the systolic peak. The location of the dicrotic notch was then detected from the APG as the location of the first local maximum before the diastolic peak.

Perfusion index was calculated using the extracted AC and DC components, and the amplitudes of the AC component were calculated using the waveform feet and peaks detected by the AMPD algorithm. DC component level changes were studied using components normalized by dividing with the initial value.

2.4. Experimental studies

The developed device was tested on 19 subjects (seven women, mean ± standard deviation age of 37 ± 13 years, range 21–68 years) with mean ± standard deviation systolic BP (SBP), MAP, DBP, and heart rate of 119 ± 17 mmHg, 93 ± 11 mmHg, 80 ± 9 mmHg, and 70 ± 9 bpm, respectively. The MAP was estimated using the simple equation of: $MAP = 1/3SBP + 2/3DBP$ [7]. Measurements were taken in a sitting position with the left arm comfortably placed on a table. A reference device (Omron M3, HEM-7154-E) was attached to the left upper arm while the finger pressure cuff was attached to the tip of the index finger of the left hand, with the PPG sensor between the volar side of the fingertip and the cuff. A measurement consisted of a series of 10 mmHg pressure steps, each lasting ten seconds. The final step was set at a suprasystolic level, typically 150 mmHg. A measurement with the reference device was taken before taking a measurement with the developed device. The process was repeated twice for each subject, resulting in 38 measurements. The study was approved by the University of Turku Ethics committee. An informed consent was obtained from all study subjects.

The gathered data was analyzed as a function of P_t instead of P_c in order to take into account the individual hemodynamics of the study participants. In this study, P_t was calculated between the MAP of the reference device attached to the upper arm and the cuff pressure of the developed device, $P_t = MAP_{ref} - P_{cuff}$. The experimental results in [23] have shown that the mean BP (MBP) measured from the fingertip using a small cuff is close to that measured from the upper arm. Our previous study with a tono-oscillometric fingertip method provided similar results [46]. Thus, the MAP of the reference device is a reasonable approximation in the P_t equation. Means and standard errors were then calculated for each P_t bin in addition to a linear regression analysis of the means to investigate the impact of P_c. The assumed model, as a function of P_t, was of the first order, $y = \beta_0 + \beta_1 x$, except in the case of green PPG amplitude and perfusion index features, where the assumed model was of the second order, $y = \beta_0 + \beta_1 x + \beta_2 x^2$ due to bell-shaped amplitude response. Moreover, coefficients of variation (CV) were calculated for PPG features to allow their comparison.

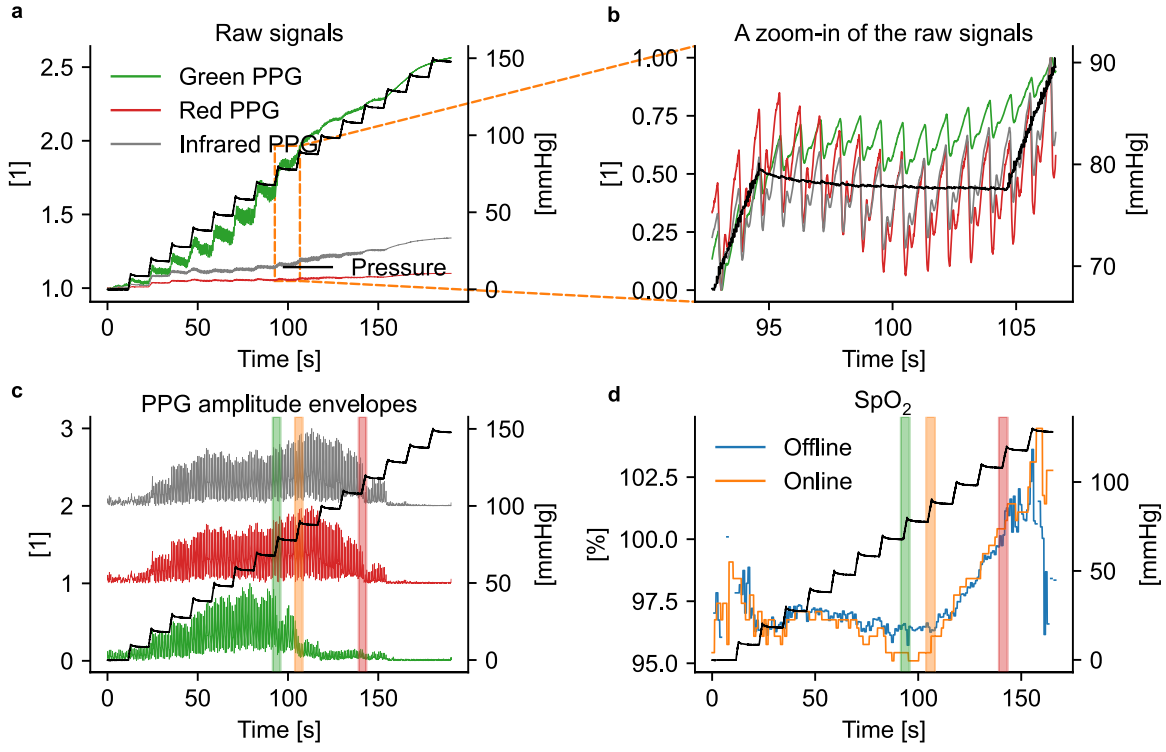

Fig. 2. An example of a measurement. The cuff pressure signal is on the right-hand side axis in all figures. a. Raw PPG signals normalized to 1 at the beginning of the measurement. The DC component of the green PPG channel changes clearly the most. b. A zoom-in of the raw signals normalized to the range [0, 1]. The signal quality is good and the individual PPG waveforms are clearly visible (note that the signals are raw, i.e. the waveforms are upside down compared to how the PPG waveforms are typically presented). c. Amplitude envelopes of the PPG signals normalized to the range [0, 1] and stacked above each other. The colors are the same as in Figure a. A clear oscillometric response can be seen in all channels. The DBP, MAP, and SBP of the reference device have been visualized in the figure as green, orange, and red bars, respectively. d. Online (calculated by the algorithm included in the device firmware while measuring) and offline (calculated after measurements) calculated SpO_2 during the measurement. Note that the highest pressure steps are omitted because the PPG channels show signs of total occlusion, and thus SpO_2 cannot be calculated.

3. Results

An example recording is presented in Fig. 2. The pressure-step nature of the measurement is clearly visible in all signals. The pressure signal is very stable within the steps, whereas the PPG signals tend to decrease slightly after a step change. The PPG signals show clear oscillometric responses with amplitudes increasing and subsequently decreasing with P_c. The red and IR channels show similar responses, whereas the green channel reaches maximum amplitude at a lower pressure level because the channel probes more superficial (lower pressure) blood vessels compared to the two longer-wavelength channels that probe deeper (higher pressure) blood vessels. The DC components, especially those of the green and IR channels, tend to increase with increasing P_c, as blood vessels are drained from the light-absorbing blood, allowing more light to be backscattered from the skin to the photodiode. The SpO_2 readings show a tendency to begin to increase at higher P_c levels.

3.1. Peripheral oxygen saturation

The linear regression analysis showed that the effect of P_c on SpO_2 was statistically significant (p value of 0.0034, ≤ 0.05) with an average change of 0.013 percentage points / mmHg in the positive P_t region. The results are further presented in Fig. 3. Despite having statistically significant relationship to P_c the SpO_2 values are rather stable at high positive P_t levels. The values begin to increase 10–20 mmHg before the DBP level and reach the theoretical maximum value of 100% slightly after MAP. The absolute maximum difference between the theoretical SpO_2 limit of 100% reached by the -10 mmHg P_t bin and the minimum value of approximately 98.1% in the 60 mmHg P_t bin is approximately 1.9 percentage points.

Fig. 3 b shows that the increase in SpO_2 values is due to the IR component in the Equation 1 increasing relative to the red component. That is, the ratio of IR AC/DC increases faster than the corresponding ratio for the red channel. Based on Fig. 3c the amplitude of the IR channel begins to increase with respect to the amplitude of the red channel slightly before the DBP level. The DC levels show a very similar pattern, as depicted in Fig. 3d.

3.2. Pulse arrival time

PATs computed using both the waveform foot and the systolic peak (PAT_{foot} and PAT_{peak}, respectively) are presented in Fig. 4. PAT_{foot} shows an increasing trend for the green PPG channel, while the red and IR channels show an increasing pattern around the level of the DBP. Interestingly, the green channel has smaller standard errors. The green PAT_{peak} shows a rather fluctuating pattern with significantly larger standard errors than in the case of PAT_{foot}. The red and IR channels then again show a rather steadily decreasing pattern after P_t 40 mmHg. Overall, the PAT_{foot}-based values show more stable and predictable patterns than those of PAT_{peak}. Table 1 shows that the effect of P_c on PAT is statistically significant in all other cases, except in the case of PAT_{peak} calculated from the green PPG signal.

The maximum differences ($PAT_{max} - PAT_{min}$) in the positive P_t region (≥ 0 mmHg) for PAT_{foot} are 25 ms, 10 ms and 9 ms for the green, red and IR channels, respectively. The values for the PAT_{peak} are 23 ms, 20 ms and 26 ms, assuming the same order of the channels. Within the same P_t range, the maximum differences between the green and IR channels are 31 ms and 58 ms for PAT_{foot} and PAT_{peak}, respectively. The higher PAT values for the green channel are expected considering that the pulse waveform travels from the deep blood vessels probed by the IR (and red) channel to the superficial blood vessels probed by the green channel. That is, the pulse waveforms recorded from the more superficial layers of the skin are delayed compared to the layers deeper in the skin.

3.3. Photoplethysmogram features

We computed several typical PPG features commonly used, for example, in diagnostics and indirect (cuffless) BP estimation techniques to study the relationship between the features and P_c and to understand the impact of the variance in these features if P_c is not controlled. These features, together with descriptions and reasonings for selection, are presented in Table 1 and further results are presented in Fig. 5. The features were grouped into four categories: i) amplitude-based, ii) temporal, iii) relative, and iv) basic. Perfusion index was categorized into amplitude-based features because the amplitude clearly dominates the feature, and, moreover, the other relative features are ratios of two similar characteristic points, whereas the perfusion index is calculated as a ratio of two vastly different things, namely the AC and DC components.

The Table 1 also presents the coefficients of variation (CV) for the features in the positive P_t region. The amplitude-based features clearly show the largest variations, while the temporal and relative features show the smallest variations. Note that the PAT_{foot} and PAT_{peak} results have been added to the table for comparison purposes, although they are not strictly PPG features. Additionally, the table presents the linear

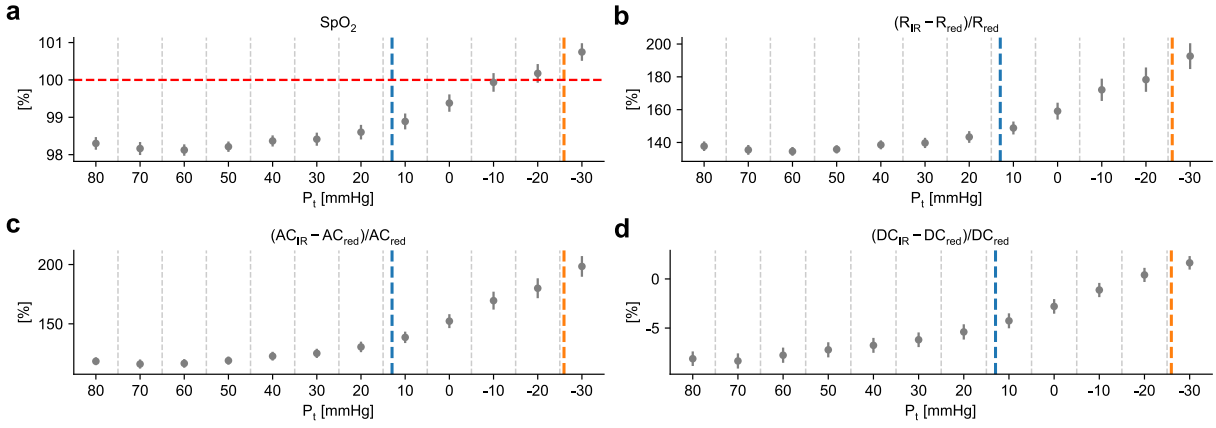

Fig. 3. SpO_2 results (mean ± standard error) as a function of P_t. The P_t bin values are center values, i.e. $P_t = 80$ mmHg covers values [85, 75), $P_t = 70$ mmHg covers values [75, 65), etc. The blue and orange vertical dashed lines mark the mean reference values of DBP and SBP, respectively. a. SpO_2 values clearly increase with increasing P_c. The horizontal red dashed line marks the theoretical maximum SpO_2 value of 100%. b. Relative red and IR component differences; $R_{red} = AC_{red} / DC_{red}$ and $R_{IR} = AC_{IR} / DC_{IR}$. The IR ratio begins to increase with respect to that of the red channel at approximately $P_t = 20$ mmHg. c. IR amplitudes begin to increase with respect to those of the red channel at around $P_t = 20$ mmHg. d. IR DC level increases rather steadily with respect to that of the red channel.

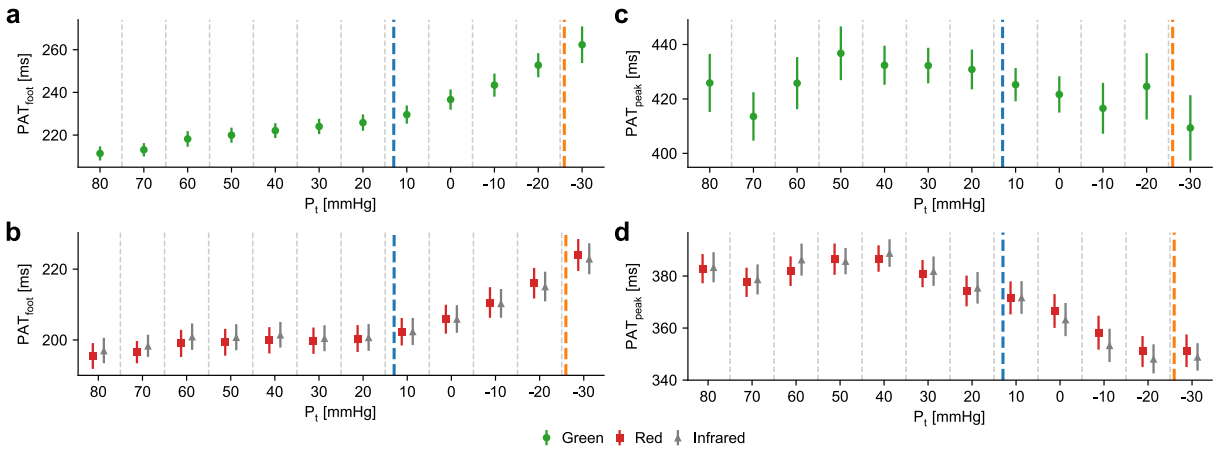

Fig. 4. PAT results (mean ± standard error) presented in a manner similar to that in Fig. 3. a. PAT_{foot} of the green channel. b. PAT_{foot} of the red and IR channels. c. PAT_{peak} of the green channel. d. PAT_{peak} of the red and IR channels.

Table 1
The calculated PPG features and their coefficients of variation (CV) and polynomial regression coefficients in the positive P_t region. The CV values are absolute, |CV| (this only matters with respect to APG b/a which has negative values). The assumed regression model was of the first order, $y = \beta_0 + \beta_1 x$, except in the case of green PPG amplitude and perfusion index features where the assumed model was of the second order, $y = \beta_0 + \beta_1 x + \beta_2 x^2$. Significant p values, $p \leq 0.05$, have been marked with an asterisk (*). The letters in parenthesis in the *feature* column refer to Fig. 1c. Note that the PAT_{foot} and PAT_{peak} values have been provided only for comparison purposes, i.e. they have not been included in the categorial mean values.

Category	Feature	Reasoning	|CV|			β_1 (p_1), β_2 (p_2)		
			Green	Red	IR	Green	Red	IR
Amplitude	Amplitude (Amp): The vertical distance between the systolic peak (S) and the waveform foot (F)	BP estimation algorithms [12,48] and usage in oscillometric measurements	0.140	0.210	0.258	9.4e-03 (8.4e-03*), -1.1e-04 (8.5e-03*)	-4.1e-03 (3.6e-06*)	-4.6e-03 (3.1e-05*)
	Perfusion index (PI): $Amp_{systole}$ / DC component level	Hemodynamic monitoring [13]	0.183	0.214	0.235	7.5e-04 (8.0e-03*), -8.0e-06 (1.3e-02*)	-4.3e-05 (2.3e-04*)	-1.1e-04 (4.0e-04*)
		Category mean	0.161	0.212	0.246			
Temporal	Crest time (CT): The time difference between the systolic peak (S) and the waveform foot (F)	Arterial stiffness [3]	0.047	0.062	0.067	3.2e-04 (3.2e-02*)	4.4e-04 (3.6e-03*)	3.9e-04 (3.4e-02*)
	ΔT: The time difference between the diastolic (D) and systolic peaks (S)	Arterial stiffness [3]	0.035	0.044	0.035	7.2e-05 (5.5e-01)	-3.2e-04 (1.6e-02*)	-1.6e-04 (1.9e-01)
	Slope transit time (STT): The slope of a line from the waveform foot (F) to the systolic peak (S)	A single point proxy for pulse transit time [1]	0.040	0.074	0.076	-3.1e-03 (1.4e-01)	-1.1e-02 (1.0e-03*)	-1.0e-02 (1.1e-02*)
		Category mean	0.040	0.060	0.059			
	PAT_{foot}: The time difference between the PPG foot (F) and the ECG R peak	BP estimation [29]	0.036	0.015	0.012	-2.8e-01 (3.6e-06*)	-1.0e-01 (2.1e-04*)	-7.8e-02 (2.8e-03*)
	PAT_{peak}: The time difference between the PPG systolic peak (S) and the ECG R peak	BP estimation [11]	0.016	0.018	0.022	-4.0e-02 (6.9e-01)	1.7e-01 (3.9e-02*)	2.1e-01 (3.3e-02*)
Relative	Reflection index (RI): $Amp_{diastole}/Amp_{systole}$	Arterial stiffness [33]	0.027	0.014	0.018	-2.4e-04 (4.5e-01)	-1.3e-04 (4.3e-01)	1.8e-04 (3.7e-01)
	Inflection point area ratio (IPA): $A_{systole}/A_{diastole}$	Total peripheral resistance [56]	0.050	0.096	0.060	-1.3e-03 (1.4e-01)	1.1e-04 (9.5e-01)	4.7e-04 (6.8e-01)
	APG b/a: The amplitude ratio of APG b (b) and a (a)	Aging and arterial stiffness [4,20,50]	0.029	0.047	0.034	-1.2e-04 (6.3e-01)	7.4e-04 (9.4e-02)	8.8e-05 (8.0e-01)
		Category mean	0.035	0.052	0.037			
Basic	DC level: PPG signal DC component level	Relation to average blood volume and tissues [2]	0.088	0.004	0.015	-3.4e-03 (1.3e-04*)	1.6e-04 (3.0e-05*)	-5.5e-04 (4.3e-05*)
		All categories mean	0.071	0.085	0.089			

regression coefficients along with their p values in the positive P_t region. In particular, the relative features show insignificant p values, indicating that they are rather insensitive to changes in P_c, as also illustrated in Fig. 5. Amplitude-based features together with the DC level expectedly show statistical significance, although in the case of the green PPG channel the relationship to P_c is non-linear compared to the red and IR channels because the channel reaches its maximum amplitude at a lower P_c level. Note that the relationship would be non-linear also for the red and IR amplitudes if all P_t bins had been used. With respect to temporal features, ΔT has statistical significance only in the red channel.

Amplitude: Expectedly, the waveform amplitudes show oscillometric responses where the amplitudes increase with increasing P_c and then subsequently decrease after the P_c has reached the MBP. For the red and IR channels, MBP is equal to MAP ($P_t = 0$) because they probe large arteries deep in the skin, but for the green channel the pressure level is lower (P_t of 30–40 mmHg) because the channel mainly probes lower pressure superficial blood vessels. Note that the IR amplitudes indeed increase more than those of the red channel, as already shown in the chapter 3.1.

Perfusion index (PI): Shows a pattern similar to amplitudes, which is quite expected considering that the perfusion index is defined as the ratio of waveform amplitude (systolic amplitude) and the DC component. It can thus be said that the amplitude is the dominant factor of the two.

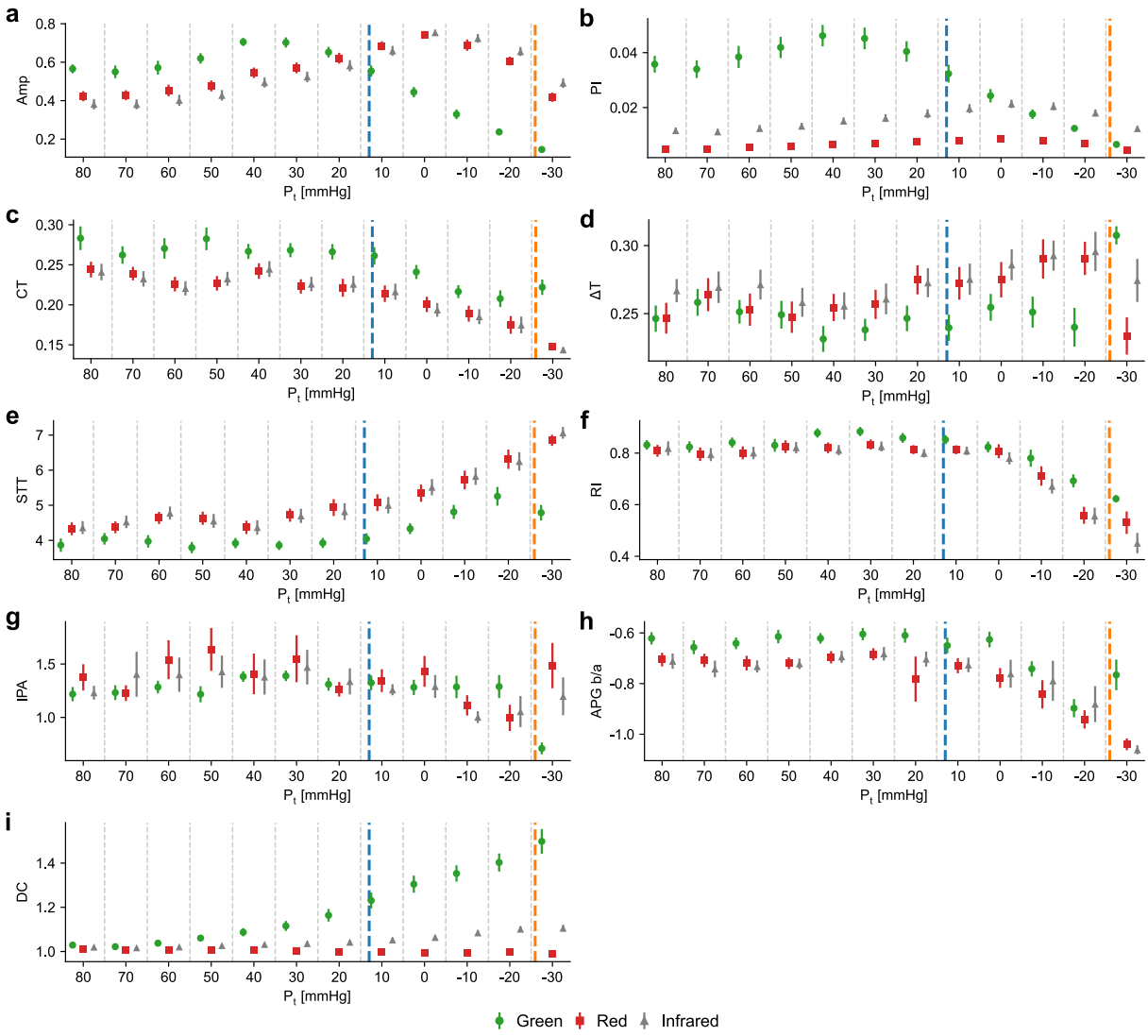

Fig. 5. Results on PPG features (mean ± standard error) presented in a manner similar to that in Fig. 3. a–b. Amplitude-based features: amplitude (a) and perfusion index (b). c–e. Temporal features: crest time (c), ΔT (d), and slope transit time (e). f–h. Relative features: reflection index (f), inflection point area ratio (g), and APG b/a (h). i. DC level (a basic feature).

Crest time (CT): Rather stable at low P_c levels but begins to steadily decrease after $P_t = 20$ mmHg. The decreasing trend means that the systolic peak moves toward the waveform foot (onset) as the P_c increases. This actually partly explains why the PAT_{peak} values showed a tendency to decrease.

ΔT*:* The response is also rather flat at low P_c levels but starts to fluctuate more approximately at $P_t = 20$ mmHg.

Slope transit time (STT): Shows an inverse response with respect to CT. This is expected considering that the STT is the slope from the waveform foot to the systolic peak, and thus the slope increases if the systolic peak moves toward the waveform foot, as indicated by CT.

Reflection index (RI): At low P_c levels, the response is rather flat but begins to decrease rapidly around the MAP. This is due to the amplitude of the diastolic peak decreasing relative to the systolic peak at high levels of P_c – a sign that blood vessels are starting to compress.

Inflection point area ratio (IPA): The response to P_c fluctuates in the positive P_t region but shows a tendency, especially in the red and IR channels, to decrease in the negative P_t region.

APG b/a: Rather stable in the positive P_t region after which there is a tendency to decrease.

DC level: The green channel shows a clearly increasing pattern with increasing P_c, as does the IR channel, although in a less significant way. The red channel shows a fairly flat, even slightly decreasing pattern with increasing P_c. The red DC component seems to vary between measurements, with some measurements showing an increasing trend and some a decreasing trend.

4. Discussion

We studied the effects of sensor P_c on MWPPG signals measured from the fingertip using a custom finger-cuff device. Varying P_c was shown to affect all parameters examined, as further discussed in the following.

4.1. Peripheral oxygen saturation

SpO_2 was found to be fairly insensitive to P_c at low pressure levels with the increasing trend starting approximately 10–20 mmHg below DBP. This is in agreement with the data provided in [15] where the mean red/IR intensity ratio starts to change at similar pressure levels. However, the reported ratio appears to stabilize after that, which is in contrast to our results. This could be because in [15] the sensor was placed on the forehead, which has less compressible soft tissue than a fingertip. In both studies, the IR amplitudes increased more than the red amplitudes with increasing P_c.

Increasing P_c has also been reported to increase the error of the SpO_2 estimates [22]. The magnitude of the error was reported to be 1–2% when P_c was approximately between 75 and 113 mmHg. This is in agreement with our results, where on average SpO_2 increased by 1.9 percentage points by the -10 mmHg P_t bin (approximately a P_c of 100 mmHg). Therefore, in general, studies seem to show that P_c affects SpO_2. Our results further show that both IR amplitudes and DC levels tend to increase relative to those of the red channel.

In [15] it was hypothesized that an increase in P_c diminishes venous blood in the tissue beneath the sensor and thus reduces its effects on signals. We tend to agree with this hypothesis in that increasing P_c is likely to push the less oxygen-rich venous blood out of the tissue with the subsequent effect of increasing the SpO_2. However, considering the low BP in the venous system, one would also expect the effects of venous blood to disappear at a fairly low P_c (as blood is pushed out), and hence, the SpO_2 values should stabilize in contrast to continuing to increase as in our results. The rather stable SpO_2 values at low P_c levels do, however, indicate that SpO_2 could be measured using, for example, a patch-like device attached to the skin with relatively low P_c.

4.2. Pulse arrival time

PAT_{foot} values were shown to be more stable than the PAT_{peak} values, especially below the level of DBP (i.e., the likely pressure region for any real application). This suggests that the waveform foot is a better choice for PAT than the waveform peak. The red and IR channels were on average more stable in the positive P_t region, although the green channel had smaller standard errors, i.e., although the green channel had an increasing trend with increasing P_c, it was quite consistent in doing so. The tendency of IR PAT_{foot} to increase around DBP is consistent with the results presented in [8], although, contrary to their results, we did not observe a U-shaped pattern before the values begin to increase. This could be due to the significantly lower sampling rate in our measurements (100 Hz vs. 1 kHz). However, we did observe the decreasing trend of IR PAT_{peak} values around the DBP as presented in [8].

The rather large difference between the PAT values of the green channel and those of the red and IR channels is due to the difference in probing depths. The pulse waveforms recorded by the green channel are delayed relative to those of the red and IR channels because the green channel probes more superficial blood vessels, whereas the red and IR channels probe more deeper arteries. This delay has been studied, for example, as a more convenient method to measure continuous BP with only a single MWPPG sensor, eliminating the need for a second sensor, such as the ECG in the case of PAT [25]. However, PAT-based methods, in general, have shown limited reliability in BP estimation [26,31].

4.3. Photoplethysmogram features

In the analysis of PPG features, the amplitude-based features expectedly had the largest variation in the positive P_t region, implying that such features are inferior in PWA unless the sensor P_c is accurately controlled. The maximum amplitude of the red and IR channels at $P_t = 0$ provides a practical P_c limit for any PPG application as the sensation of maximally pulsating large arteries is rather unpleasant, not to mention ischemia as P_c approaches SBP. Overall, the relative features had the lowest variation, although there was only a small difference compared to the temporal features.

When comparing the wavelengths, the green channel had the lowest overall variation, whereas the red channel had a slightly smaller variation than the IR channel. However, this comparison is not entirely fair. The green channel probes superficial lower-pressure blood vessels, and thus benefits in the variation calculation from the fact that its amplitude maximum occurs at a lower pressure level than those of the red and IR channels, which probe deeper higher-pressure blood vessels. Considering that amplitude-based features show significantly greater variation than the rest of the categories, we also made the same comparison while ignoring the amplitude category altogether. In this case, the channels show negligible differences over the remaining features.

Sensor P_c might have a significant impact on the clinical interpretation of the PPG features. For example, our results showed that APG b/a, that is used as an index of arterial stiffness (e.g., vascular modifications due to aging), begins to increase when P_c approaches MAP and has significant changes after that, in line with the results in [18]. We used the linear regression model presented in [50] to estimate the age from the IR APG b/a ratio by using the variation range of [-0.76, -0.68] in the positive P_t region (see Fig. 5). This led to an age range of [33, 43] years, a difference of ten years. That is, if the APG b/a ratio had been used to estimate the age of a study subject, the age (a proxy for arterial stiffness) would have varied by ten years depending only on the P_c. Although the APG b/a ratio showed relatively small variation (see Table 1) and statistically insignificant linear regression coefficient, the relationship to age in this case, was fairly large. It is reasonable to expect that similar large variations in the final interpretation of the other features are possible. Thus, the effect of sensor P_c on PPG features might be significant. Based on Fig. 5, to minimize this effect, it is best to keep the sensor P_c below the level of the DBP. In a practical application, a slight contact pressure of approximately 20–30 mmHg is recommended to avoid excessive movement artifacts.

4.4. Limitations and future directions

The results clearly show that sensor P_c affects all studied PPG-derived parameters, highlighting the need to give P_c appropriate importance in PPG device designs. It is also important to note that the effect of sensor P_c is dependent on the MAP, and therefore even with an optimal P_c, the effective P_t is subject to change depending on the varying arterial pressure. Therefore, ways to take into account the hemodynamics of an individual, ideally dynamically, rather than measuring absolute P_c, could be helpful in some cases. This could be achieved by finding ways to control or measure P_c in different measurement setups. A major limitation of the current study is its study population, which consisted of only healthy study subjects. More research is needed to understand the effects of P_c on PPG signals in critically ill and diseased patients. Additionally, the developed device was unable to detect the faint arterial pulsations in the cuff pressure due to the relatively large air volume, leaving an interesting comparison of the PPG parameters with the respective cuff pressure signal parameters unexplored.

5. Conclusion

We presented a finger-cuff-based device to measure MWPPG (green, red, and IR) signals at different sensor P_c levels. The signals were analyzed in terms of (i) SpO_2, (ii) PAT, and (iii) PPG features. Increasing sensor P_c to approximately the level of MAP increased SpO_2 values by approximately 1.9 percentage points in our healthy study population, driven by the IR component. PAT values calculated using the waveform foot, especially those of the red and IR channels, were found to be more reliable than those calculated using the waveform peak. PPG features should be recorded at sensor P_c levels between a slight P_c (20–30 mmHg) and the level of DBP, and amplitude-based features should be avoided. In conclusion, uncontrolled sensor P_c is a source of inaccuracy in PPG applications, and thus P_c should be given more consideration.

CRediT authorship contribution statement

Jukka-Pekka Sirkiä: Writing – original draft, Writing – review & editing, Validation, Visualization, Supervision, Software, Resources, Project administration, Methodology, Investigation, Funding acquisition, Formal analysis, Data curation, Conceptualization. **Tuukka Panula:** Writing – original draft, Writing – review & editing, Visualization, Methodology, Funding acquisition, Conceptualization. **Matti Kaisti:** Writing – review & editing, Writing – original draft, Visualization,

Validation, Supervision, Resources, Project administration, Methodology, Conceptualization.

Declaration of competing interest

The authors declare that they have no known competing financial interests or personal relationships that could have appeared to influence the work reported in this paper.

Data availability

The data used are available from the corresponding author on reasonable request.

Acknowledgement

The works of J.-P.S. and T.P. were supported by the University of Turku Graduate School.

References

[1] P.S. Addison, Slope transit time (STT): a pulse transit time proxy requiring only a single signal fiducial point, IEEE Trans. Biomed. Eng. 63 (11) (2016) 2441–2444, https://doi.org/10.1109/TBME.2016.2528507.
[2] J. Allen, Photoplethysmography and its application in clinical physiological measurement, Physiol. Measur. 28 (2007) R1–39, https://doi.org/10.1088/0967-3334/28/3/R01.
[3] S.R. Alty, N. Angarita-Jaimes, S.C. Millasseau, P.J. Chowienczyk, Predicting arterial stiffness from the digital volume pulse waveform, IEEE Trans. Biomed. Eng. 54 (12) (2007) 2268–2275, https://doi.org/10.1109/TBME.2007.897805.
[4] H.J. Baek, J.S. Kim, Y.S. Kim, H.B. Lee, K.S. Park, Second derivative of photoplethysmography for estimating vascular aging. 2007 6th International Special Topic Conference on Information Technology Applications in Biomedicine, 2007, pp. 70–72, https://doi.org/10.1109/ITAB.2007.4407346.
[5] M. Basza, D. Wałąg, W. Kowalczyk, A. Bożym, M. Ciurla, M. Krzyżanowska, C. Maciejewski, W. Bojanowicz, M. Soliński, Ł. Kołtowski, Photoplethysmography wave morphology in patients with atrial fibrillation, Physiol. Measur. 44 (4) (2023) 045001, https://doi.org/10.1088/1361-6579/acc725.
[6] M. Bester, M.J. Almario Escorcia, P. Fonseca, M. Mollura, M.M. van Gilst, R. Barbieri, M. Mischi, J.O.E.H. van Laar, R. Vullings, R. Joshi, The impact of healthy pregnancy on features of heart rate variability and pulse wave morphology derived from wrist-worn photoplethysmography, Sci. Rep. 13 (1) (2023) 21100, https://doi.org/10.1038/s41598-023-47980-2.
[7] W.J. Bos, E. Verrij, H.H. Vincent, B.E. Westerhof, G. Parati, G.A. van Montfrans, How to assess mean blood pressure properly at the brachial artery level, J. Hypertension 25 (4) (2007) 751, https://doi.org/10.1097/HJH.0b013e32803fb621.
[8] A. Chandrasekhar, M. Yavarimanesh, K. Natarajan, J.-O. Hahn, R. Mukkamala, PPG sensor contact pressure should be taken into account for cuff-less blood pressure measurement, IEEE Trans. Bio-Med. Eng. 67 (11) (2020) 3134–3140, https://doi.org/10.1109/TBME.2020.2976989.
[9] P.H. Charlton, B. Paliakaitė, K. Pilt, M. Bachler, S. Zanelli, D. Kulin, J. Allen, M. Hallab, E. Bianchini, C.C. Mayer, D. Terentes-Printzios, V. Dittrich, B. Hametner, D. Veerasingam, D. Žikić, V. Marozas, Assessing hemodynamics from the photoplethysmogram to gain insights into vascular age: a review from VascAgeNet, Am. J. Physiol.-Heart Circulat. Physiol. 322 (4) (2022) H493–H522, https://doi.org/10.1152/ajpheart.00392.2021.
[10] P.H. Charlton, K. Pilt, P.A. Kyriacou, Establishing best practices in photoplethysmography signal acquisition and processing, Physiol. Measur. 43 (5) (2022) 050301, https://doi.org/10.1088/1361-6579/ac6cc4.
[11] Y. Choi, Q. Zhang, S. Ko, Noninvasive cuffless blood pressure estimation using pulse transit time and Hilbert–Huang transform, Comput. Electric. Eng. 39 (1) (2013) 103–111, https://doi.org/10.1016/j.compeleceng.2012.09.005.
[12] E.C.-P. Chua, S.J. Redmond, G. McDarby, C. Heneghan, Towards using photoplethysmogram amplitude to measure blood pressure during sleep, Annal. Biomed. Eng. 38 (3) (2010) 945–954, https://doi.org/10.1007/s10439-009-9882-z.
[13] M. Coutrot, E. Dudoignon, J. Joachim, E. Gayat, F. Vallée, F. Dépret, perfusion index: physical principles, physiological meanings and clinical implications in anaesthesia and critical care, Anaesthesia Crit. Care Pain Med. 40 (6) (2021) 100964, https://doi.org/10.1016/j.accpm.2021.100964.
[14] L. D'Acquisto, F. Scardulla, N. Montinaro, S. Pasta, Z. Daniele, D. Bellavia, A preliminary investigation of the effect of contact pressure on the accuracy of heart rate monitoring by wearable PPG wrist band, 2019, pp. 334–338, https://doi.org/10.1109/METROI4.2019.8792834.
[15] A.C.M. Dassel, R. Graaff, M. Sikkema, A. Meijer, W.G. Zijlstra, J.G. Aarnoudse, Reflectance pulse oximetry at the forehead improves by pressure on the probe, J. Clin. Monitor. 11 (4) (1995) 237–244, https://doi.org/10.1007/BF01617518.
[16] M. Elgendi, On the analysis of fingertip photoplethysmogram signals, Curr. Cardiol. Rev. 8 (1) (2012) 14–25, https://doi.org/10.2174/157340312801215782.
[17] E. Finnegan, S. Davidson, M. Harford, P. Watkinson, L. Tarassenko, M. Villarroel, Features from the photoplethysmogram and the electrocardiogram for estimating changes in blood pressure, Sci. Rep. 13 (1) (2023) 986, https://doi.org/10.1038/s41598-022-27170-2.
[18] A. Grabovskis, Z. Marcinkevics, U. Rubins, E. Kviesis-Kipge, Effect of probe contact pressure on the photoplethysmographic assessment of conduit artery stiffness, J. Biomed. Opt. 18 (2) (2013) 027004, https://doi.org/10.1117/1.JBO.18.2.027004.
[19] Guidelines for SpO2 measurement | analog devices, (https://www.analog.com/en/technical-articles/guidelines-for-spo2-measurement–maxim-integrated.html).
[20] I. Imanaga, H. Hara, S. Koyanagi, K. Tanaka, Correlation between wave components of the second derivative of plethysmogram and arterial distensibility, Japanese Heart J. 39 (6) (1998) 775–784, https://doi.org/10.1536/ihj.39.775.
[21] J.-H. Lee, S. Yang, J. Park, H.C. Kim, E.-H. Kim, Y.-E. Jang, J.-T. Kim, H.-S. Kim, Time to consider the contact force during photoplethysmography measurement during pediatric anesthesia: A prospective, nonrandomized interventional study, Pediatric Anesthesia 28 (7) (2018) 660–667, https://doi.org/10.1111/pan.13415.
[22] C. Liu, R. Correia, H.K. Ballaji, S. Korposh, B.R. Hayes-Gill, S.P. Morgan, Optical fibre-based pulse oximetry sensor with contact force detection, Sensors 18 (11) (2018) 3632, https://doi.org/10.3390/s18113632.
[23] J. Liu, C.G. Sodini, Y. Ou, B. Yan, Y.-T. Zhang, N. Zhao, Feasibility of fingertip oscillometric blood pressure measurement: model-based analysis and experimental validation, IEEE J. Biomed. Health Inf. 24 (2) (2020) 533–542, https://doi.org/10.1109/JBHI.2019.2919896.
[24] J. Liu, B. Yan, S.-C. Chen, Y.-T. Zhang, C. Sodini, N. Zhao, Non-invasive capillary blood pressure measurement enabling early detection and classification of venous congestion, IEEE J. Biomed. Health Inf. 25 (8) (2021) 2877–2886, https://doi.org/10.1109/JBHI.2021.3055760.
[25] J. Liu, B.P. Yan, Y.-T. Zhang, X.-R. Ding, P. Su, N. Zhao, Multi-wavelength photoplethysmography enabling continuous blood pressure measurement with compact wearable electronics, IEEE Trans. Biomed. Eng. 66 (6) (2019) 1514–1525, https://doi.org/10.1109/TBME.2018.2874957.
[26] Z.-D. Liu, Y. Li, Y.-T. Zhang, J. Zeng, Z.-X. Chen, Z.-W. Cui, J.-K. Liu, F. Miao, Cuffless blood pressure measurement using smartwatches: a large-scale validation study, IEEE J. Biomed. Health Inf. 27 (9) (2023) 4216–4227, https://doi.org/10.1109/JBHI.2023.3278168.
[27] J.M. May, E. Mejía-Mejía, M. Nomoni, K. Budidha, C. Choi, P.A. Kyriacou, Effects of contact pressure in reflectance photoplethysmography in an in vitro tissue-vessel phantom, Sensors (Basel, Switzerland) 21 (24) (2021) 8421, https://doi.org/10.3390/s21248421.
[28] E. Mejía-Mejía, J. Allen, K. Budidha, C. El-Hajj, P.A. Kyriacou, P.H. Charlton, 4 - Photoplethysmography signal processing and synthesis, in: J. Allen, P. Kyriacou (Eds.), Photoplethysmography, Academic Press, 2022, pp. 69–146, https://doi.org/10.1016/B978-0-12-823374-0.00015-3.
[29] R. Mukkamala, J.-O. Hahn, O.T. Inan, L.K. Mestha, C.-S. Kim, H. Töreyin, S. Kyal, Toward ubiquitous blood pressure monitoring via pulse transit time: theory and practice, IEEE Trans. Biomed. Eng. 62 (8) (2015) 1879–1901, https://doi.org/10.1109/TBME.2015.2441951.
[30] J. Pan, W.J. Tompkins, A real-time QRS detection algorithm, IEEE Trans. Biomed. Eng. BME-32 (3) (1985) 230–236, https://doi.org/10.1109/TBME.1985.325532.
[31] T. Panula, J.-P. Sirkiä, D. Wong, M. Kaisti, Advances in non-invasive blood pressure measurement techniques, IEEE Rev. Biomed. Eng. 16 (2023) 424–438, https://doi.org/10.1109/RBME.2022.3141877.
[32] J. Park, H.S. Seok, S.-S. Kim, H. Shin, Photoplethysmogram analysis and applications: an integrative review, Front. Physiol. 12 (2022).
[33] K. Pilt, K. Meigas, R. Ferenets, K. Temitski, M. Viigimaa, Photoplethysmographic signal waveform index for detection of increased arterial stiffness, Physiol. Measur. 35 (10) (2014) 2027, https://doi.org/10.1088/0967-3334/35/10/2027.
[34] D. Ray, T. Collins, S.I. Woolley, P.V.S. Ponnapalli, A review of wearable multi-wavelength photoplethysmography, IEEE Rev. Biomed. Eng. 16 (2023) 136–151, https://doi.org/10.1109/RBME.2021.3121476.
[35] RD117_MBED - MBED firmware for MAXREFDES117 Heart Rate / SpO2... | Mbed, (https://os.mbed.com/teams/Maxim-Integrated/code/RD117_MBED/).
[36] A. Reisner, P.A. Shaltis, D. McCombie, H.H. Asada, D.S. Warner, M.A. Warner, Utility of the photoplethysmogram in circulatory monitoring, Anesthesiology 108 (5) (2008) 950–958, https://doi.org/10.1097/ALN.0b013e31816c89e1.
[37] S. Rhee, B.-H. Yang, H. Asada, Artifact-resistant power-efficient design of finger-ring plethysmographic sensors, IEEE Trans. Biomed. Eng. 48 (7) (2001) 795–805, https://doi.org/10.1109/10.930904.
[38] E. Sabeti, N. Reamaroon, M. Mathis, J. Gryak, M. Sjoding, K. Najarian, Signal quality measure for pulsatile physiological signals using morphological features: applications in reliability measure for pulse oximetry, Inf. Med. Unlock. 16 (2019) 100222, https://doi.org/10.1016/j.imu.2019.100222.
[39] P. Santos, V. Almeida, J. Cardoso, C. Correia, Photoplethysmographic logger with contact force and hydrostatic pressure monitoring. 2013 IEEE 3rd Portuguese Meeting in Bioengineering (ENBENG), 2013, pp. 1–6, https://doi.org/10.1109/ENBENG.2013.6518437.
[40] F. Scardulla, G. Cosoli, S. Spinsante, A. Poli, G. Iadarola, R. Pernice, A. Busacca, S. Pasta, L. Scalise, L. D'Acquisto, Photoplethysmograhic sensors, potential and limitations: Is it time for regulation? A comprehensive review, Measurement 218 (2023) 113150, https://doi.org/10.1016/j.measurement.2023.113150.
[41] F. Scardulla, L. D'Acquisto, R. Colombarini, S. Hu, S. Pasta, D. Bellavia, A study on the effect of contact pressure during physical activity on photoplethysmographic

heart rate measurements, Sensors 20 (18) (2020) 5052, https://doi.org/10.3390/s20185052.
[42] F. Scholkmann, J. Boss, M. Wolf, An efficient algorithm for automatic peak detection in noisy periodic and quasi-periodic signals, Algorithms 5 (4) (2012) 588–603, https://doi.org/10.3390/a5040588.
[43] K.H. Shelley, D. Tamai, D. Jablonka, M. Gesquiere, R.G. Stout, D.G. Silverman, The effect of venous pulsation on the forehead pulse oximeter wave form as a possible source of error in Spo2 calculation, Anesthesia Analgesia 100 (3) (2005) 743, https://doi.org/10.1213/01.ANE.0000145063.01043.4B.
[44] H. Shin, S.D. Min, Feasibility study for the non-invasive blood pressure estimation based on ppg morphology: normotensive subject study, BioMed. Eng. OnLine 16 (1) (2017) 10, https://doi.org/10.1186/s12938-016-0302-y.
[45] J.K. Sim, B. Ahn, I. Doh, A contact-force regulated photoplethysmography (PPG) platform, AIP Adv. 8 (4) (2018) 045210, https://doi.org/10.1063/1.5020914.
[46] J.-P. Sirkiä, T. Panula, M. Kaisti, Tonometric multi-wavelength photoplethysmography for studying the cutaneous microvasculature of the fingertip, IEEE Trans. Instrument. Measur. 72 (2023) 1–13, https://doi.org/10.1109/TIM.2023.3293873.
[47] J. Spigulis, L. Gailite, R. Erts, A. Lihachev, Contact probe pressure effects in skin multi-spectral photoplethysmography - art. no. 66281F, Progr. Biomed. Opt. Imag. - Proc. SPIE 6628 (2007), https://doi.org/10.1117/12.727985.
[48] S. Sun, E. Bresch, J. Muehlsteff, L. Schmitt, X. Long, R. Bezemer, I. Paulussen, G. J. Noordergraaf, R.M. Aarts, Systolic blood pressure estimation using ECG and PPG in patients undergoing surgery, Biomed. Signal Process. Control 79 (2023) 104040, https://doi.org/10.1016/j.bspc.2022.104040.
[49] Y. Sun, N. Thakor, Photoplethysmography revisited: from contact to noncontact, from point to imaging, IEEE Trans. Biomed. Eng. 63 (3) (2016) 463–477, https://doi.org/10.1109/TBME.2015.2476337.
[50] K. Takazawa, N. Tanaka, M. Fujita, O. Matsuoka, T. Saiki, M. Aikawa, S. Tamura, C. Ibukiyama, Assessment of vasoactive agents and vascular aging by the second derivative of photoplethysmogram waveform, Hypertension 32 (2) (1998) 365–370, https://doi.org/10.1161/01.HYP.32.2.365.
[51] T. Tamura, Current progress of photoplethysmography and SPO2 for health monitoring, Biomed. Eng. Lett. 9 (1) (2019) 21–36, https://doi.org/10.1007/s13534-019-00097-w.
[52] T. Tamura, Y. Maeda, M. Sekine, M. Yoshida, Wearable photoplethysmographic sensors—past and present, Electronics 3 (2) (2014) 282–302, https://doi.org/10.3390/electronics3020282.
[53] X.F. Teng, Y.T. Zhang, The effect of contacting force on photoplethysmographic signals, Physiol. Measur. 25 (5) (2004) 1323, https://doi.org/10.1088/0967-3334/25/5/020.
[54] X.F. Teng, Y.T. Zhang, The effect of applied sensor contact force on pulse transit time, Physiol. Measur. 27 (8) (2006) 675, https://doi.org/10.1088/0967-3334/27/8/002.
[55] X.-F. Teng, Y.-T. Zhang, Theoretical study on the effect of sensor contact force on pulse transit time, IEEE Trans. Bio-Med. Eng. 54 (8) (2007) 1490–1498, https://doi.org/10.1109/TBME.2007.900815.
[56] L. Wang, E. Pickwell-MacPherson, Y.P. Liang, Y.T. Zhang, Noninvasive cardiac output estimation using a novel photoplethysmogram index. 2009 Annual International Conference of the IEEE Engineering in Medicine and Biology Society, 2009, pp. 1746–1749, https://doi.org/10.1109/IEMBS.2009.5333091.
[57] K. Yamakoshi, P. Rolfe, C. Murphy, Current developments in non-invasive measurement of arterial blood pressure, J. Biomed. Eng. 10 (2) (1988) 130–137, https://doi.org/10.1016/0141-5425(88)90088-X.
[58] K.I. Yamakoshi, H. Shimazu, T. Togawa, Indirect measurement of instantaneous arterial blood pressure in the rat, Am. J. Physiol.-Heart Circulat. Physiol. 237 (5) (1979) H632–H637, https://doi.org/10.1152/ajpheart.1979.237.5.H632.
[59] K.-I. Yamakoshi, H. Shimazu, T. Togawa, Indirect measurement of instantaneous arterial blood pressure in the human finger by the vascular unloading technique, IEEE Trans. Biomed. Eng. BME-27 (3) (1980) 150–155, https://doi.org/10.1109/TBME.1980.326616.
[60] Y.L. Yang, H.S. Seok, G.-J. Noh, B.-M. Choi, H. Shin, Postoperative pain assessment indices based on photoplethysmography waveform analysis, Front. Physiol. 9 (2018).